

Highly Tunable Spin-Orbit Torque and Anisotropic Magnetoresistance in a Topological Insulator Thin Film Attached to Ferromagnetic Layer

Ali G. Moghaddam^{1,2,3,*}, Alireza Qaiumzadeh⁴, Anna Dyrdał⁵, and Jamal Berakdar³

¹Department of Physics, Institute for Advanced Studies in Basic Sciences (IASBS), Zanjan 45137-66731, Iran

²Research Center for Basic Sciences and Modern Technologies (RBST), Institute for Advanced Studies in Basic Science (IASBS), Zanjan 45137-66731, Iran

³Institut für Physik, Martin-Luther Universität Halle-Wittenberg, D-06099 Halle, Germany

⁴Center for Quantum Spintronics, Department of Physics, Norwegian University of Science and Technology, NO-7491 Trondheim, Norway

⁵Faculty of Physics, Adam Mickiewicz University, Uniwersytetu Poznańskiego 2, 61-614 Poznań, Poland



(Received 24 February 2020; accepted 7 October 2020; published 5 November 2020)

We investigate spin-charge conversion phenomena in hybrid structures of topological insulator thin films and magnetic insulators. We find an anisotropic inverse spin-galvanic effect that yields a highly tunable spin-orbit torque. Concentrating on the quasiballistic limit, we also predict a giant anisotropic magnetoresistance at low dopings. These effects, which have no counterparts in thick topological insulators, depend on the simultaneous presence of the hybridization between the surface states and the in-plane magnetization. Both the inverse spin-galvanic effect and anisotropic magnetoresistance exhibit a strong dependence on the magnetization and the Fermi level position and can be used for spintronics and spin-orbit-torque-based applications at the nanoscale.

DOI: [10.1103/PhysRevLett.125.196801](https://doi.org/10.1103/PhysRevLett.125.196801)

Introduction.—The discovery of new types of topological phases and topological insulators (TIs) [1–7] has opened up a new line of fundamental research with prospective applications in electronic and optical devices [1,2]. Spin-related phenomena are at the heart of TIs [8–10] due to the *spin-momentum locking* property of their surface states as gapless excitations protected by time-reversal symmetry [1,2,11]. With these properties, TIs can be used to convert pure spin excitation as a carrier of information into an electric (charge) signal or to electrically control magnetization [12–25]. In most previous studies, only out-of-plane magnetizations effectively influenced the surface states through the generation of a Dirac mass term [12,13,16,18]. Large spin-orbit torques (SOTs) and the resulting magnetization switching have been demonstrated for hybrid magnetic TI structures [26–33]. Other studies have reported the reciprocal effect of spin-electricity signal conversion and spin pumping with an exceptionally large efficiency [34–37].

In this Letter, we predict a new feature for thin TIs attached to ferromagnetic (FM) layers with in-plane magnetization: when the thickness of the TI approaches a few quintuple layers, the surface states at the two sides start hybridizing, and a band gap opens in the surface state spectrum even without a perturbation that breaks the time-reversal symmetry [38–46]. Intriguingly, we find that the average of the in-plane magnetizations can also modify the energy dispersion of the surface states. This is surprising because, for nonhybridized TI surfaces (e.g., for thicker

films), the in-plane components of magnetization can be gauged away [47–51], and they do not contribute to effects such as gap opening [52–56]. Then, as a key finding, we illustrate that the interplay of hybridization with the in-plane magnetization significantly influences the SOTs originating from the inverse spin-galvanic effect (ISGE) [18,57] and the anisotropic magnetoresistance (AMR). For a certain range of chemical potentials feasible for experiments, the current-induced spin densities exhibit large anisotropy, and AMR becomes very prominent. Also, the strong dependence of the spin densities on the magnetization and the chemical potential yield a magneto-electrically controllable SOT with a nonlinear magnetization dependence that can be used in TI-based spintronic devices, SOT nano-oscillators [58,59], and even neuro-morphic computing, which was recently proposed [60].

Model.—We consider a TI thin film with a nanometer-scale thickness, d , coupled to one or two adjacent FM layers with magnetizations \mathbf{m}_{\pm} , as schematically shown in Fig. 1. Assuming Dirac-like surface states at the two sides with hybridization energy Δ , the effective low-energy Hamiltonian of the system is [46–49,61]

$$\mathcal{H} = v_F \tau_z \otimes (\hat{\mathbf{z}} \times \boldsymbol{\sigma}) \cdot (\mathbf{p} - \tau_z \boldsymbol{\kappa} - \boldsymbol{\kappa}_0) + \Delta \tau_x \otimes \sigma_0, \quad (1)$$

where v_F denotes the Fermi velocity of the surface states, and the Pauli matrices σ_i and τ_i act in the spin and layer subspaces, respectively. Two types of momentum shifts $\boldsymbol{\kappa} = (g/2v_F) \sum_{\zeta} \mathbf{m}_{\zeta} \times \hat{\mathbf{z}}$ and $\boldsymbol{\kappa}_0 = (g/2v_F) \sum_{\zeta} \zeta \mathbf{m}_{\zeta} \times \hat{\mathbf{z}}$

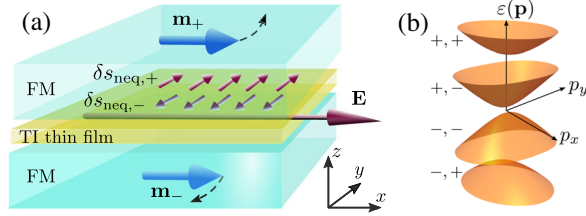


FIG. 1. The device setup and its band structure. (a) Schematic of a TI thin film sandwiched between two FM layers. The ISGE leads to nonequilibrium spin densities perpendicular to the applied electric field that have opposite directions on the two surfaces of the thin film. (b) Band dispersion of the thin film assuming $v_F\kappa/\Delta = 0.9$. The band labeling is according to the text in the form of a double index (ν, η) .

originate from the exchange coupling $\mathcal{H}_{\text{ex}} = g \sum_{\zeta} \boldsymbol{\sigma} \cdot \mathbf{m}_{\zeta}(1 + \zeta\tau_z)/2$ between the TI surface states and the magnetization of the adjacent FM layers on top of and beneath the thin film ($\zeta = \pm$ represent the two sides of the surface states). The global momentum shift κ_0 is equivalent to the rigid movement of the full energy bands and can be simply gauged away without any physical consequences. In contrast, the layer-dependent momentum shifts $\pm\kappa$ due to the coupling Δ cannot be gauged out, and as we will see, they radically influence the transport properties of the hybridized surface states [62].

Current-induced spin densities.—The ISGE or non-equilibrium spin density driven by the charge current originates from spin-orbit coupling. In TI thin films, the opposite helicities of the surface states at the two sides imply that the current-induced spin densities at the two surfaces also have opposite signs ($\delta s_{\text{neq},-} = -\delta s_{\text{neq},+}$). Thus, in the linear response, the spin densities are related to the external electric field \mathbf{E} as $\delta s_{\text{neq},\zeta}^i = \zeta(-e) \sum_j \mathcal{S}_{ij} E_j$, in which \mathcal{S} is a second-rank pseudotensor defining the *ISGE response function* (i.e., spin susceptibility). According to the Středa–Smrčka version of the Kubo formula [63–65], the components of \mathcal{S} have two contributions related to the Fermi surface and the completely filled energy levels (Fermi sea):

$$\mathcal{S}_{ij}^I = \Re \int \frac{d\epsilon d^2\mathbf{p}}{(2\pi)^3} \partial_{\epsilon} f(\epsilon) \text{Tr}[\hat{s}_{i,+} \hat{G}_{\epsilon}^R \hat{v}_j (\hat{G}_{\epsilon}^R - \hat{G}_{\epsilon}^A)], \quad (2)$$

$$\begin{aligned} \mathcal{S}_{ij}^{\text{II}} = \Re \int \frac{d\epsilon d^2\mathbf{p}}{(2\pi)^3} f(\epsilon) \text{Tr}[\hat{s}_{i,+} \hat{G}_{\epsilon}^R \hat{v}_j \partial_{\epsilon} \hat{G}_{\epsilon}^R \\ - \hat{s}_{i,+} \partial_{\epsilon} \hat{G}_{\epsilon}^R \hat{v}_j \hat{G}_{\epsilon}^R]. \end{aligned} \quad (3)$$

Here, $f(\epsilon)$ is the Fermi–Dirac distribution function, and $G_{\epsilon}^{R,A}$ denote the momentum space retarded and advanced Green’s functions [the momentum \mathbf{p} is dropped from $G^{R,A}(\mathbf{p})$ for brevity]. Additionally, $\hat{s}_{\zeta} = (\tau_0 + \zeta\tau_z) \otimes \boldsymbol{\sigma}/2$ and $\hat{v} = v_F\tau_z \otimes \boldsymbol{\sigma}$ are the surface-dependent spin operator and velocity operator, respectively. By replacing $s_{i,+}$ in

Eqs. (2) and (3) with $s_{i,-}$, both functions \mathcal{S}_{ij}^I and $\mathcal{S}_{ij}^{\text{II}}$ also change sign, justifying the appearance of prefactor ζ in the linear response relation for the spin densities. In addition, the lack of a nontrivial topology and Berry-phase-attributed effects, which is a consequence of the hybridization of the surface states, implies that the contribution from the Fermi sea is negligible [66,67], and therefore, $\mathcal{S} = \mathcal{S}^I$.

The noninteracting Green’s function for the clean system defined by Hamiltonian Eq. (1) is

$$\hat{G}_{0\omega}^{R,A}(\mathbf{p}) = \frac{1}{\omega \pm i0^+ - \hat{\mathcal{H}}} = \sum_{\nu,\eta} \frac{\hat{\mathcal{P}}_{\nu,\eta}(\mathbf{p})}{\omega \pm i0^+ - \epsilon_{\nu,\eta}(\mathbf{p})}, \quad (4)$$

in which $\hat{\mathcal{P}}_{\nu,\eta}(\mathbf{p}) = |\psi_{\nu,\eta}(\mathbf{p})\rangle\langle\psi_{\nu,\eta}(\mathbf{p})|$ is the projection operator to eigenstate $|\psi_{\nu,\eta}(\mathbf{p})\rangle$. As illustrated in Fig. 1(b), we have four energy bands $\epsilon_{\nu,\eta}(\mathbf{p}) = \nu[v_F^2 p_x^2 + (v_F\kappa + \eta\sqrt{v_F^2 p_y^2 + \Delta^2})^2]^{1/2}$, with indices ν and η taking two values ± 1 . The projection operators are the sum of the two terms [61]

$$\begin{aligned} \hat{\mathcal{P}}_{\nu,\eta}^{\text{(even)}}(\mathbf{p}) = \frac{1}{4} [\tau_0\sigma_0 - \nu \cos\theta_{\eta}\tau_0\sigma_x \\ - \eta \text{sech}\xi(\tau_x\sigma_x - \nu \cos\theta_{\eta}\tau_x\sigma_0)], \end{aligned} \quad (5)$$

$$\begin{aligned} \hat{\mathcal{P}}_{\nu,\eta}^{\text{(odd)}}(\mathbf{p}) = \frac{\nu}{4} [\sin\theta_{\eta}\tau_z\sigma_y - \eta \text{sech}\xi \sin\theta_{\eta}\tau_y\sigma_z \\ - \eta \tanh\xi(\nu\tau_z\sigma_0 - \cos\theta_{\eta}\tau_z\sigma_x + \sin\theta_{\eta}\tau_0\sigma_y)], \end{aligned} \quad (6)$$

which are even and odd functions of the momentum. Parameters $\xi = \arcsin h(v_F p_y/\Delta)$ and $\theta_{\eta} = \arcsin[-v_F p_x/\epsilon_{+,\eta}(\mathbf{p})]$ are used for brevity.

In the presence of disorder, we expect a level broadening matrix $\hat{\Gamma}_{\omega}$ represented by the imaginary part of the corresponding self-energy function $\hat{\Sigma}_{\omega}$. Considering short-range impurities with an effective constant potential V_0 and a density n_{imp} , the level broadening can be expressed within the Born approximation (BA) as

$$\begin{aligned} \hat{\Gamma}_{\omega} = \Im \Sigma_{\omega}^{\text{BA}} = n_{\text{imp}} V_0^2 \int \frac{d^2\mathbf{p}}{(2\pi\hbar)^2} \Im \hat{G}_{0\omega}^R(\mathbf{p}), \\ = -\frac{\gamma}{\pi} \int v_F^2 d^2\mathbf{p} \sum_{\nu,\eta} \delta[\omega - \nu\epsilon_{\eta}(\mathbf{p})] \Re \hat{\mathcal{P}}_{\nu,\eta}(\mathbf{p}), \end{aligned} \quad (7)$$

in which the dimensionless impurity scattering strength is given by $\gamma = n_{\text{imp}} V_0^2 / (2\hbar v_F)^2$. By integration over momentum, only even terms $\mathcal{P}_{\nu,\eta}^{\text{(even)}}(\mathbf{p})$ do not vanish; therefore, one obtains the decomposed form $\hat{\Gamma}_{\omega} = \sum_{i,j=0,1} \Gamma_{ij} \tau_i \otimes \sigma_j$, following from Eq. (5). Interestingly, due to their similar matrix structure, the terms Γ_{00} , Γ_{01} , and Γ_{10} can be absorbed into ω , κ , and Δ in the expressions for the retarded Green’s function:

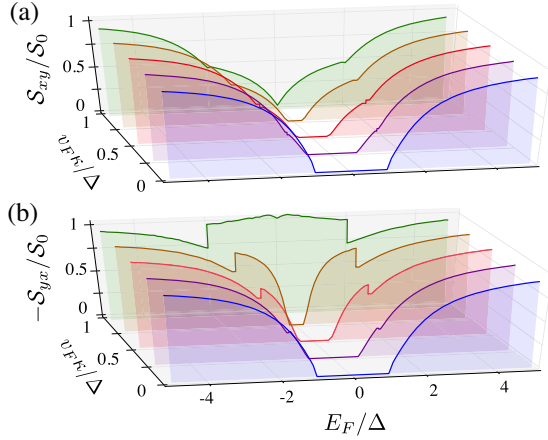


FIG. 2. Energy dependence of the transverse spin-current response functions (a) S_{xy} and (b) S_{yx} at zero temperature and for different magnetic momentum shifts κ . Finite values of κ give rise to anisotropy in the spin-current response, which becomes profound for $v_F\kappa \sim \Delta$. Here, we have used $\gamma = 0.1$ for the effective disorder strength.

$$\hat{G}_\omega^R(\mathbf{p}) = [\omega - \hat{\mathcal{H}} - i\hat{\Gamma}_\omega]^{-1} = [\tilde{\omega} - \tilde{\mathcal{H}} - i\hat{\Gamma}'_\omega]^{-1}, \quad (8)$$

with the substitutions $\tilde{\mathcal{H}}[\kappa, \Delta] \equiv \mathcal{H}[\kappa - i\Gamma_{01}/v_F, \Delta + i\Gamma_{10}]$, $\tilde{\omega} = \omega - i\Gamma_{00}$, and $\hat{\Gamma}'_\omega = \Gamma_{11}\tau_1 \otimes \sigma_1$. The advanced Green's function follows from $\hat{G}_\omega^A = \hat{G}_\omega^{R*}$.

Numerical results and discussion.—Combining Eq. (8) for $\hat{G}_\omega^{R,A}(\mathbf{p})$ with Eq. (2), taking the zero temperature limit with $\partial_\varepsilon f(\varepsilon) = -\delta(\varepsilon)$, and numerically performing the integration, the Fermi level contribution to the spin-current response function S_{ij}^l is obtained. We immediately see that only off-diagonal terms S_{xy} and S_{yx} are nonvanishing, as expected from the chiral form of the low-energy surface state spectrum. Intriguingly, from Fig. 2, the amplitudes of the two components of the spin-current response function can be quite different, indicating the anisotropic nature of the current-induced nonequilibrium spin density. In fact, the anisotropy of the energy bands that originates from the magnetic momentum shift κ causes a marked difference between S_{xy} and S_{yx} . This difference is particularly evident for the range of Fermi energies $|E_F - \Delta| < v_F|\kappa|$, that is, when only one band crosses the Fermi energy. When the Fermi energy falls inside the gap [$E_F < (\Delta - v_F|\kappa|)$], the induced spin densities identically vanish. In contrast, for large energies, the anisotropy becomes negligible, and the spin-current responses monotonically increase, approaching a constant value $S_0 = 1/(8\pi v_F\gamma)$ for $E_F \gg \Delta$, $v_F|\kappa|$ [61].

Assuming a weak scattering regime ($\gamma \ll 1$), we find that the spin-current responses decline with the disorder strength as $1/\gamma$, which resembles a conductivitylike behavior. In fact, a relationship between the off-diagonal spin-charge response functions and the diagonal components of the conductivity matrix as $S_{xy} = (\hbar/2e^2v_F)\sigma_{xx}$ and $S_{yx} = -(\hbar/2e^2v_F)\sigma_{yy}$, which has been previously

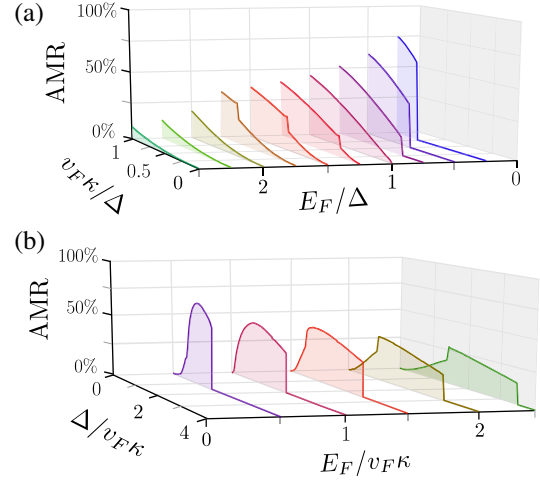


FIG. 3. Variation in the AMR (the percentage of the relative difference between the two components of the longitudinal resistance) with (a) the magnetization of the FM layer and (b) the hybridization of surface states for various values of the Fermi energy. Note that both horizontal axes in panel (a) have reversed directions for the sake of clarity of the results.

found for a single surface of a TI [12,13], also holds for coupled surfaces. Therefore, anisotropic behavior similar to that shown in Figs. 2(a) and 2(b) is expected for the magnetoconductivities. Figure 3(a) presents the variation in the AMR with κ (note that κ defines the magnetization in energy units, $v_F\kappa = gm/2$) and the chemical potential. A very large AMR is achieved for small chemical potentials compared to both the hybridization and magnetic energy scales ($E_F \ll \Delta$, $v_F|\kappa|$). For a fixed chemical potential with respect to Δ , the AMR is generally an ascending function of magnetization. Additionally, the AMR vanishes inside the band gap and abruptly changes when the number of bands crossing the Fermi level changes. As a result, both the gap width and the splitting between bands of a TI thin film coupled to an FM layer (or in the presence of a magnetic field) can be determined by measuring the AMR. It should be stressed that in Fig. 3, only positive chemical potentials and magnetizations are shown, but due to the symmetry, the same behavior can be expected when changing the sign of each or both of them. Now, as illustrated in Fig. 2(b) for weak overlaps ($\Delta < v_F\kappa$), the AMR is small, and upon approaching $\Delta = 0$, it vanishes. This is indeed consistent with the fact that, for completely isolated surface states, the opposite momentum shifts $\pm\kappa$ can be independently gauged away [61], and therefore, we do not expect any anisotropy.

Associated with the nonequilibrium spin densities, the SOT exerted on the two magnetizations on opposite sides can be obtained from $\boldsymbol{\tau}_{\text{SOT},\zeta} = (g/\hbar)\mathbf{m}_\zeta \times \delta\mathbf{s}_{\text{neq},\zeta}$. Then, by choosing the local coordinates such that the in-plane magnetization aligns in the $+\hat{x}$ direction, as shown in Fig. 1, we use the above results for the spin-current response functions and obtain the SOT as follows:

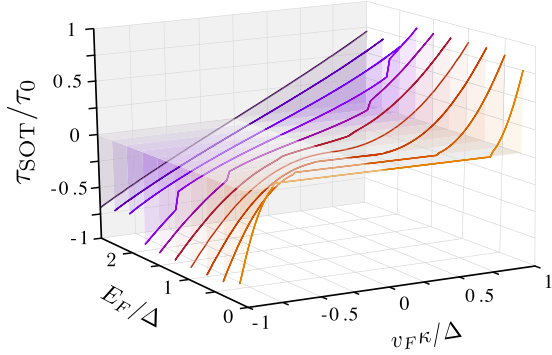


FIG. 4. Variation in the SOT (scaled by $\tau_0 = 2eE_{\parallel}\Delta\mathcal{S}_0/\hbar$) with the magnetization of the FM layer for various values of the Fermi energy of the TI thin film. For smaller Fermi energies ($E_F/\Delta \lesssim 1$), the SOT vanishes for the range of magnetic exchange energies $gm/2 \equiv v_F\kappa$, where the Fermi level lies inside a gap, and then starts to increase in a nonlinear manner above a certain value. At higher energies, the nonlinearity becomes negligible.

$$\boldsymbol{\tau}_{\text{SOT},\zeta} = -\frac{\zeta ge}{\hbar} \mathbf{m}_{\zeta} \cdot \mathbf{E} \mathcal{S}_{yx} \hat{\mathbf{z}}. \quad (9)$$

Note that \mathcal{S}_{yx} is a function of the magnetizations due to the momentum shift $\boldsymbol{\kappa}$, i.e., $\mathcal{S}_{yx} = \mathcal{S}_{yx}(\sum_{\zeta'} \mathbf{m}_{\zeta'})$. This result is in agreement with the general form of the Rashba SOT in two-dimensional systems, especially when only in-plane magnetization is considered [68,69]. Nevertheless, the explicit form of the magnetization dependence is particularly different from those obtained in bulk TI coupled to FM layers when the band gap is opened by the out-of-plane component of the magnetization [18].

The variation in the SOT with the magnetization and Fermi energy is shown in Fig. 4. Similar to the AMR, the SOT exhibits a significant behavioral change when the Fermi energy moves from the energy gap into the first conduction or valence subbands or reaches the edge of the second conduction or valence bands, suggesting that the band gap and band splitting can be inferred from the Fermi energy dependence of the SOT. Importantly, for sufficiently small Fermi energies $E_F \lesssim \Delta$, the SOT nonlinearly varies with the magnetization direction \mathbf{m}_{ζ} , which is a direct consequence of the dependence of \mathcal{S}_{yx} on $\boldsymbol{\kappa}$. Therefore, the results of Fig. 4 reveal that the SOT in the TI thin film can be magnetoelectrically tailored, which means that one can substantially tune the SOT and magnetic dynamics by changing both the equilibrium magnetization (its amplitude and angle) and the chemical potential via a gate voltage. This result indicates further advantageous features of FM-TI hybrid structures for spintronics and magnetization reversal applications, particularly in comparison to recent elaborate proposals [70,71].

The particular advantage of a TI thin film depends on the interplay of the in-plane magnetization and the surface state hybridization, which is manifested in the built-in

anisotropy and nonlinearity of the SOT given by Eq. (9). Various experiments and *ab initio* calculations have already indicated $\Delta \sim 10\text{--}100$ meV for thicknesses of a few quintuple layers [38,72–74]. Also, surface gaps due to the out-of-plane magnetization have been reported to vary from a few to 50 meV in magnetically doped TIs [52–54]. Therefore, combined with the Fermi level tunability by doping and external gating, our findings should be experimentally realizable, especially for the parameter range $E_F \sim \Delta \sim v_F\kappa$.

Throughout the Letter, we have focused on in-plane magnetizations to highlight their role in the thin film limit of FM-TI hybrids. The addition of out-of-plane components does not influence the anisotropy of the bands; instead, this addition augments the tunability of the transport properties by changing the band splittings. As a consequence, the qualitative features of ISGE, SOT, and AMR remain intact, although they change quantitatively. Moreover, a damping-like SOT term arises as $\boldsymbol{\tau}_{\text{SOT},\zeta}^{\parallel} = -(\zeta ge/\hbar) \hat{\mathbf{z}} \cdot \mathbf{m}_{\zeta} \mathcal{S}_{yx} \mathbf{E}$, which has been extensively explored in the case of thick TI coupled to FM [16–18,26–31].

Conclusions.—In this Letter, we have revealed unprecedented transport features of FM-TI thin films, namely large anisotropy and a strong dependence on doping in current-induced nonequilibrium spin densities and the resulting spin-orbit torques. These effects originate from the role of exchange coupling in the in-plane magnetization in the presence of a finite overlap between the surface states, which has been overlooked until now. We further predict a very large AMR in the low doping limit, which diminishes for thick TI structures with negligible hybridization of the surface states. Given that both the SOT and the AMR depend on the doping and the magnetization, the hybrids of FM and TI thin films offer promising applications in spintronics and SOT-based devices.

A. G. M. acknowledges financial support from the German Research Foundation (DFG) through Grant No. SFB TRR 227 and thanks MLU Halle-Wittenberg for the hospitality during his visit. A. Q. has been supported by the European Research Council via Advanced Grant No. 669442 “Insulatronics,” the Research Council of Norway through its Centres of Excellence funding scheme, Project No. 262633, “QuSpin.” A. D. acknowledges the financial support from the National Science Center in Poland (NCN) Project No. DEC-2018/31/D/ST3/02351.

*Corresponding author.
agorbanz@iasbs.ac.ir

- [1] M. Z. Hasan and C. L. Kane, *Rev. Mod. Phys.* **82**, 3045 (2010).
- [2] X.-L. Qi and S.-C. Zhang, *Rev. Mod. Phys.* **83**, 1057 (2011).
- [3] C.-K. Chiu, J. C. Y. Teo, A. P. Schnyder, and S. Ryu, *Rev. Mod. Phys.* **88**, 035005 (2016).

- [4] F. D. M. Haldane, *Rev. Mod. Phys.* **89**, 040502 (2017).
- [5] E. Witten, *Rev. Mod. Phys.* **88**, 035001 (2016).
- [6] B. Keimer and J. Moore, *Nat. Phys.* **13**, 1045 (2017).
- [7] Y. Ando, *J. Phys. Soc. Jpn.* **82**, 102001 (2013).
- [8] W. Han, Y. Otani, and S. Maekawa, *npj Quantum Mater.* **3**, 27 (2018).
- [9] Y. Tokura, K. Yasuda, and A. Tsukazaki, *Nat. Rev. Phys.* **1**, 126 (2019).
- [10] L. Šmejkal, Y. Mokrousov, B. Yan, and A. H. MacDonald, *Nat. Phys.* **14**, 242 (2018).
- [11] A. Soumyanarayanan, N. Reyren, A. Fert, and C. Panagopoulos, *Nature (London)* **539**, 509 (2016).
- [12] I. Garate and M. Franz, *Phys. Rev. Lett.* **104**, 146802 (2010).
- [13] T. Yokoyama, J. Zang, and N. Nagaosa, *Phys. Rev. B* **81**, 241410(R) (2010).
- [14] K. Nomura and N. Nagaosa, *Phys. Rev. B* **82**, 161401(R) (2010).
- [15] Y. Tserkovnyak and D. Loss, *Phys. Rev. Lett.* **108**, 187201 (2012).
- [16] A. Sakai and H. Kohno, *Phys. Rev. B* **89**, 165307 (2014).
- [17] M. H. Fischer, A. Vaezi, A. Manchon, and E.-A. Kim, *Phys. Rev. B* **93**, 125303 (2016).
- [18] P. B. Ndiaye, C. A. Akosa, M. H. Fischer, A. Vaezi, E.-A. Kim, and A. Manchon, *Phys. Rev. B* **96**, 014408 (2017).
- [19] A. Manchon, J. Železný, I. M. Miron, T. Jungwirth, J. Sinova, A. Thiaville, K. Garello, and P. Gambardella, *Rev. Mod. Phys.* **91**, 035004 (2019).
- [20] S. Zhang and A. Fert, *Phys. Rev. B* **94**, 184423 (2016).
- [21] S. Ghosh and A. Manchon, *Phys. Rev. B* **97**, 134402 (2018).
- [22] C. S. Ho, Y. Wang, Z. B. Siu, S. G. Tan, M. B. Jalil, and H. Yang, *Sci. Rep.* **7**, 792 (2017).
- [23] Y. J. Ren, W. Y. Deng, H. Geng, R. Shen, L. B. Shao, L. Sheng, and D. Y. Xing, *Europhys. Lett.* **120**, 57004 (2017).
- [24] J.-Y. Li, R.-Q. Wang, M.-X. Deng, and M. Yang, *Phys. Rev. B* **99**, 155139 (2019).
- [25] Y.-T. Hsu, K. Park, and E.-A. Kim, *Phys. Rev. B* **96**, 235433 (2017).
- [26] A. Mellnik, J. Lee, A. Richardella, J. Grab, P. Mintun, M. H. Fischer, A. Vaezi, A. Manchon, E.-A. Kim, N. Samarth *et al.*, *Nature (London)* **511**, 449 (2014).
- [27] Y. Fan, P. Upadhyaya, X. Kou, M. Lang, S. Takei, Z. Wang, J. Tang, L. He, L.-T. Chang, M. Montazeri *et al.*, *Nat. Mater.* **13**, 699 (2014).
- [28] Y. Wang, P. Deorani, K. Banerjee, N. Koirala, M. Brahlek, S. Oh, and H. Yang, *Phys. Rev. Lett.* **114**, 257202 (2015).
- [29] Y. Fan, X. Kou, P. Upadhyaya, Q. Shao, L. Pan, M. Lang, X. Che, J. Tang, M. Montazeri, K. Murata *et al.*, *Nat. Nanotechnol.* **11**, 352 (2016).
- [30] K. Kondou, R. Yoshimi, A. Tsukazaki, Y. Fukuma, J. Matsuno, K. Takahashi, M. Kawasaki, Y. Tokura, and Y. Otani, *Nat. Phys.* **12**, 1027 (2016).
- [31] J. Han, A. Richardella, S. A. Siddiqui, J. Finley, N. Samarth, and L. Liu, *Phys. Rev. Lett.* **119**, 077702 (2017).
- [32] D. Mahendra, R. Grassi, J.-Y. Chen, M. Jamali, D. R. Hickey, D. Zhang, Z. Zhao, H. Li, P. Quarterman, Y. Lv *et al.*, *Nat. Mater.* **17**, 800 (2018).
- [33] N. H. D. Khang, Y. Ueda, and P. N. Hai, *Nat. Mater.* **17**, 808 (2018).
- [34] Y. Shiomi, K. Nomura, Y. Kajiwara, K. Eto, M. Novak, K. Segawa, Y. Ando, and E. Saitoh, *Phys. Rev. Lett.* **113**, 196601 (2014).
- [35] M. Jamali, J. S. Lee, J. S. Jeong, F. Mahfouzi, Y. Lv, Z. Zhao, B. K. Nikolic, K. A. Mkhoyan, N. Samarth, and J.-P. Wang, *Nano Lett.* **15**, 7126 (2015).
- [36] A. Baker, A. Figueroa, L. Collins-McIntyre, G. Van Der Laan, and T. Hesjedal, *Sci. Rep.* **5**, 7907 (2015).
- [37] J.-C. Rojas-Sánchez, S. Oyarzún, Y. Fu, A. Marty, C. Vergnaud, S. Gambarelli, L. Vila, M. Jamet, Y. Ohtsubo, A. Taleb-Ibrahimi, P. Le Fèvre, F. Bertran, N. Reyren, J.-M. George, and A. Fert, *Phys. Rev. Lett.* **116**, 096602 (2016).
- [38] Y. Zhang, K. He, C.-Z. Chang, C.-L. Song, L.-L. Wang, X. Chen, J.-F. Jia, Z. Fang, X. Dai, W.-Y. Shan *et al.*, *Nat. Phys.* **6**, 584 (2010).
- [39] J. Linder, T. Yokoyama, and A. Sudbø, *Phys. Rev. B* **80**, 205401 (2009).
- [40] H.-Z. Lu, W.-Y. Shan, W. Yao, Q. Niu, and S.-Q. Shen, *Phys. Rev. B* **81**, 115407 (2010).
- [41] C.-X. Liu, H. Zhang, B. Yan, X.-L. Qi, T. Frauenheim, X. Dai, Z. Fang, and S.-C. Zhang, *Phys. Rev. B* **81**, 041307(R) (2010).
- [42] H.-Z. Lu and S.-Q. Shen, *Phys. Rev. B* **84**, 125138 (2011).
- [43] S. S. Pershoguba and V. M. Yakovenko, *Phys. Rev. B* **86**, 165404 (2012).
- [44] S. S. Pershoguba, D. S. L. Abergel, V. M. Yakovenko, and A. V. Balatsky, *Phys. Rev. B* **91**, 085418 (2015).
- [45] A. Sulaev, M. Zeng, S.-Q. Shen, S. K. Cho, W. G. Zhu, Y. P. Feng, S. V. Ereemeev, Y. Kawazoe, L. Shen, and L. Wang, *Nano Lett.* **15**, 2061 (2015).
- [46] P. Ghaemi, R. S. K. Mong, and J. E. Moore, *Phys. Rev. Lett.* **105**, 166603 (2010).
- [47] A. A. Zyuzin, M. D. Hook, and A. A. Burkov, *Phys. Rev. B* **83**, 245428 (2011).
- [48] F. Parhizgar, A. G. Moghaddam, and R. Asgari, *Phys. Rev. B* **92**, 045429 (2015).
- [49] V. Litvinov, *Magnetism in Topological Insulators* (Springer, Cham, 2020).
- [50] T. Chiba, S. Takahashi, and G. E. W. Bauer, *Phys. Rev. B* **95**, 094428 (2017).
- [51] A. Dyrdał, J. Barnaś, and A. Fert, *Phys. Rev. Lett.* **124**, 046802 (2020).
- [52] Y. Chen, J.-H. Chu, J. Analytis, Z. Liu, K. Igarashi, H.-H. Kuo, X. Qi, S.-K. Mo, R. Moore, D. Lu *et al.*, *Science* **329**, 659 (2010).
- [53] L. A. Wray, S.-Y. Xu, Y. Xia, D. Hsieh, A. V. Fedorov, Y. San Hor, R. J. Cava, A. Bansil, H. Lin, and M. Z. Hasan, *Nat. Phys.* **7**, 32 (2011).
- [54] I. Lee, C. K. Kim, J. Lee, S. J. L. Billinge, R. Zhong, J. A. Schneeloch, T. Liu, T. Valla, J. M. Tranquada, G. Gu, and J. C. S. Davis, *Proc. Natl. Acad. Sci. U.S.A.* **112**, 1316 (2015).
- [55] S.-Y. Xu, M. Neupane, C. Liu, D. Zhang, A. Richardella, L. A. Wray, N. Alidoust, M. Leandersson, T. Balasubramanian, J. Sánchez-Barriga *et al.*, *Nat. Phys.* **8**, 616 (2012).
- [56] G. J. Ferreira and D. Loss, *Phys. Rev. Lett.* **111**, 106802 (2013).
- [57] V. M. Edelstein, *Solid State Commun.* **73**, 233 (1990).

- [58] T. Chen, R. K. Dumas, A. Eklund, P. K. Muduli, A. Houshang, A. A. Awad, P. Drrenfeld, B. G. Malm, A. Rusu, and J. kerman, *Proc. IEEE* **104**, 1919 (2016).
- [59] M. Haidar, A. A. Awad, M. Dvornik, R. Khymyn, A. Houshang, and J. Å kerman, *Nat. Commun.* **10**, 2362 (2019).
- [60] J. Torrejon, M. Riou, F. A. Araujo, S. Tsunegi, G. Khalsa, D. Querlioz, P. Bortolotti, V. Cros, K. Yakushiji, A. Fukushima *et al.*, *Nature (London)* **547**, 428 (2017).
- [61] See Supplemental Material at <http://link.aps.org/supplemental/10.1103/PhysRevLett.125.196801> for more details and derivation.
- [62] Detailed explanation of the gauge invariance and symmetry properties of the model can be found in the first section of the Supplemental Material [61].
- [63] L. Smrčka and P. Sředa, *J. Phys. C* **10**, 2153 (1977).
- [64] P. Sředa, *J. Phys. C* **15**, L717 (1982).
- [65] N. A. Sinitsyn, J. E. Hill, H. Min, J. Sinova, and A. H. MacDonald, *Phys. Rev. Lett.* **97**, 106804 (2006).
- [66] A. Dyrdał, J. Barnaś, and V. K. Dugaev, *Phys. Rev. B* **95**, 245302 (2017).
- [67] S. Kudła, A. Dyrdał, V. K. Dugaev, J. Berakdar, and J. Barnaś, *Phys. Rev. B* **100**, 205428 (2019).
- [68] I. A. Ado, O. A. Tretiakov, and M. Titov, *Phys. Rev. B* **95**, 094401 (2017).
- [69] I. A. Ado, P. M. Ostrovsky, and M. Titov, *Phys. Rev. B* **101**, 085405 (2020).
- [70] M. Rodriguez-Vega, G. Schwiete, J. Sinova, and E. Rossi, *Phys. Rev. B* **96**, 235419 (2017).
- [71] M. F. Maghrebi, A. V. Gorshkov, and J. D. Sau, *Phys. Rev. Lett.* **123**, 055901 (2019).
- [72] Y. Jiang, Y. Wang, M. Chen, Z. Li, C. Song, K. He, L. Wang, X. Chen, X. Ma, and Q.-K. Xue, *Phys. Rev. Lett.* **108**, 016401 (2012).
- [73] T. Zhang, J. Ha, N. Levy, Y. Kuk, and J. Stroschio, *Phys. Rev. Lett.* **111**, 056803 (2013).
- [74] M. Kim, C. H. Kim, H.-S. Kim, and J. Ihm, *Proc. Natl. Acad. Sci. U.S.A.* **109**, 671 (2012).